Available online at www.eccomasproceedia.org
Eccomas Proceedia SMART (2025) 1154-1169

ECCOMAS
Proceedia

XI ECCOMAS Thematic Conference on Smart Structures and Materials - SMART 2025
M. Krommer, M. Nader and M. Schagerl (Eds)

Received: 1 April 2025 / Revised: 29 August 2025 / Accepted: 10 September 2025

Morphing Aircraft Wing Structure for the Application of 3D Shock Control Bumps

Sven Christian Künnecke, Martin Radestock, Hans Peter Monner

Abstract. The increasing demand for efficient and adaptable aircraft designs leads to the development of morphing structures, which can alter their shape in response to changing flight conditions. In this study, the design of a hybrid wing skin structure made of a fiber composite laminate and an elastomer is described. The primary goal is to develop a shape-variable structure that can be actively transformed into a shock control bump. As conventional aircraft operate at transonic speeds, a shockwave forms on the wing upper side, leading to wave drag and increased overall drag. Introducing a shock control bump aims to reduce the shock's intensity, thereby mitigating its detrimental effects on drag. In contrast to former structural studies, this bump has a three-dimensional (3D) shape, and thus, the morphing skin section is mounted on all sides. Consequently, the shape-variable structure is designed to allow such complex deformations. A comprehensive sensitivity study is conducted, exploring the impact of composite as well as elastomer design parameters. The results of this study reveal a structural feasible wing skin design that can be deformed to a 3D shock control bump. The proposed design demonstrates potential for application in real-world aircraft designs, offering a promising solution for mitigating transonic shock effects on wing performance and reducing overall drag.

Key words: Morphing aircraft structure, adaptive aircraft, morphing wing, shape-variable fiber composite, transonic shock control, hybrid structure

1 INTRODUCTION

The aviation sector is driven by the pressing need to meet European sustainability targets. In light of goals such as the European Green Deal [1] or the Flightpath 2050 [2], the industry is increasingly focused on minimizing its carbon footprint, with particular attention given to reducing fuel consumption and greenhouse gas emissions. Consequently, there is a growing recognition that innovative technologies must play a central role in ensuring that aviation reduces its environmental impact. One promising technological approach in this context is the

Sven Christian Künnecke & Martin Radestock & Hans Peter Monner
German Aerospace Center (DLR), Institute of Lightweight Systems, Lilienthalplatz 7, 38108 Braunschweig, Germany, e-mail: Sven.Kuennecke@DLR.de

ISSN:3078-543X. Published by Eccomas Proceedia.
Peer-review under responsibility of the organizing committee of SMART 2025.
doi: 10.7712/150125.13709.303002

development of advanced morphing structures for aircraft, which offer the potential for significant aerodynamic improvements. Morphing components, such as droop noses, trailing edges, and spoilers [3, 4, 5, 6, 7, 8, 9], can adjust their shape in response to changing flight conditions, thereby optimizing performance throughout different phases of flight. Morphing concepts have been the subject of numerous studies, where Barbarino et al. (2011) [10] provide a comprehensive review.

A particularly critical challenge in modern commercial aviation is handling the aerodynamic effects of transonic flow. During cruise, most conventional transport aircraft experience transonic conditions, where the airflow over the wing reaches speeds close to the speed of sound, resulting in the formation of a transonic shock wave. This shock induces wave drag, which contributes to a significant increase in fuel consumption [11, 12] and can even lead to undesirable aerodynamic phenomena, such as buffet [13, 14]. The need for strategies to mitigate the adverse effects of this shock is, therefore, a central concern in the pursuit of more fuel-efficient and environmentally friendly aircraft.

One of the most widely studied concepts for mitigating transonic shocks is the use of shock control bumps (SCBs), which were first introduced by Ashill et al. (1992) [15]. SCBs are devices placed on the surface of an aircraft wing in the vicinity of the shock, designed to influence the flow field and lower the shock strength. By altering the pressure distribution over the wing, these bumps can reduce wave drag [11, 12, 16] and even delay the buffet onset [11, 13, 14, 17], leading to improved aerodynamic performance. An extensive review on SCBs has been conducted by Bruce and Colliss (2015) [18]. For further details especially regarding the aerodynamic effects of these devices, the reader is referred to this paper.

Besides two-dimensional (2D) SCBs [11, 12, 14, 16, 18], 3D bumps have been investigated in recent years [13, 17, 18, 19, 20, 21]. According to [18], 2D bumps often exhibit poor off-design performance, whereas 3D SCBs can be applied to a broader operational range since they maintain their effectiveness over wider ranges of Mach numbers and angles of attack. The desirable so-called λ-shock structure is generated by both, 2D and 3D SCBs. However, a decay

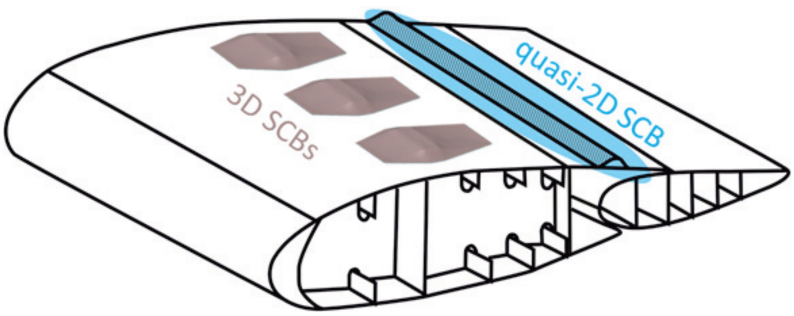

Figure 1: Exemplary illustration of an quasi-2D SCB and 3D SCBs on an aircraft wing without consideration of a specific shock position

in spanwise direction is visible for the 3D variants. According to Ogawa et al. (2008) [19], this spanwise decay of the shock structure is gradual and can be compensated by placing adjacent 3D bumps in such a way that overlapping shock structures are formed. This can lead to a quasi-2D shock structure and thus mitigate potential negative effects of the finite 3D devices. An exemplary illustration of 2D and 3D SCBs is depicted in figure 1.

To provide clarity of terminology related to 2D and 3D SCBs, “infinite“ is referring to 2D bumps that are considered over the entire span of an infinite wing. In other words, this is a theoretical construct. Previous studies utilize structural pre-bends on morphing spoilers [8, 9, 22] or pressurized chambers [5, 6, 7] to form an SCB over the entire spoiler span. Since the bump shape is maintained on the spoiler tips, these SCBs are categorized as “quasi-2D“ because they are not truly infinite due to their restriction withing the spoiler geometries, but are also not entirely finite in the sense of 3D SCBs.

Rigid SCBs remain fixed in position and shape, as they are permanently attached to the wing. Such devices would not be able to adapt to the dynamic conditions of flight. Fixed bumps could potentially lead to an increase in drag under off-design conditions, such as during takeoff and landing or when they are not optimally positioned relative to the shock location. This is why already in the project EUROSHOCK II [11] adaptive bumps have aerodynamically been investigated.

In recent years, studies on structural designs of morphing SCBs have been conducted. Several of these are summarized by Künnecke et al. (2021) [23]. Besides the above mentioned SCB concepts on morphing spoilers, flexible plates have been investigated that are installed above a cavity on the wing upper side [21, 24]. These plates can be passively deformed by aerodynamic pressure and further supported by actuators to create either 2D or 3D SCBs. However, these structural concepts are limited in producing complex 3D shapes but primarily yield hill-like bumps with smooth transitions between bump shape and the surrounding wing surface.

In this work, a complex 3D SCB shape is investigated which poses challenges in terms of structural design, especially on the flanks of the bump. While a quasi-2D bump on a morphing spoiler can be realized by using a sliding contact on the trailing edge flap due to the free spoiler chordwise end [8, 9, 22], a 3D bump has a finite span and thus, all side edges are fixed. Consequently, large deformations on a small area are necessary to deploy the SCB. Such high strains that become necessary for the formation of 3D bumps cannot be handled with a pure fiber composite structure. Therefore, in this work, a hybrid skin concept that combines elastomer and fiberglass materials is developed and the structural design is simulated in finite element analyses.

2 FINITE ELEMENT ANALYSIS

A finite element analysis (FEA) model is set up in ANSYS Workbench. For this purpose, a parametric computer-aided design (CAD) model has been created. This geometry is imported into the ANSYS Workbench environment and a script-based interface for automatically building

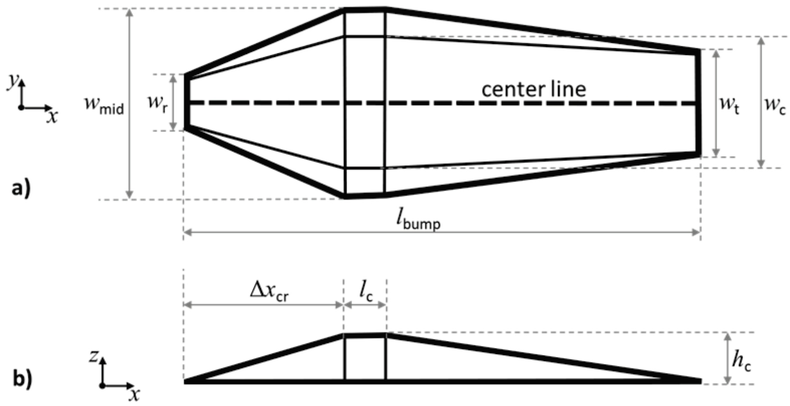

Figure 2: Parametrization in top view a) and side view b) of the 3D SCB for performance increase via wave drag reduction based on [17]

the structural model using the ANSYS tools ACP-Pre and Mechanical is developed.

The 3D SCB parametrization that serves as target shape in this work has been taken from Mayer at al. (2018) [17]. The considered bump shape is applied for the performance-optimized configuration, thus leading to wave drag reduction. This parametrization of the 3D performance bump is depicted in figure 2.

The prescribed parameters in [17] are summarized in table 1. Since the structural design of the morphing skin for such a 3D bump is the focus of this work, the parameters given in table 1 are taken as target values an not changed. These values are given in percent of the wing chord length (%c) at the respective spanwise section.

Mayer et al. [17] investigate two design points, which result in different optimized values of the bump parameters for both cases. In this work, the parameters of the design point which leads to the highest bump in [17] are considered. Consequently, a bump height (h_{c}) of 1.15%c is taken as target height. The corresponding distance from the bump leading edge to the beginning of the crest plateau (Δx_{cr}) is determined from the parameters in [17] and amount to 8.8%c. For details about the aerodynamic conditions on which the parameters in table 1 are based on, the reader is referred to [17].

Table 1: Parameters of a 3D performance SCB based on [17]

l_{bump}	l_{c}	w_{r}	w_{mid}	w_{c}	w_{t}	Δx_{cr}	h_{c}
25%c	3%c	6%c	10%c	6%c	6%c	8.8%c	1.15%c

2.1 Material models

In previous studies on morphing spoilers [8, 9, 22], a flexible glass-fiber reinforced polymer (GFRP) ply-stacking has been implemented which is based on [25]. However, such a spoiler structure is design for a quasi-2D SCB with a free downstream bump end that is equal to the spoiler trailing edge. In a 3D bump design, all sides of the flexible bump are fixed in a comparatively stiff surrounding wing skin structure, thus requiring the morphing skin to handle the deformations and strains itself. Due to the high deformations that occur over a small area, resulting in large strains, it is not possible to realize a pure GFRP structure. Therefore, a hybrid structural design has been defined, consisting of GFRP and an elastomer. This elastomer is an ethylene propylene diene monomer (EPDM), a synthetic rubber that can endure large strains of several hundred percent [26], while the max. strains for GFRP are about single-digit percent.

Table 2: Material properties of GFRP and EPDM based on [25, 27, 28]

Material	Properties	Material model in FEA
EPDM	G_0 = 1.9 MPa $d = 1 \cdot 10^{-9}$ Pa^{-1}	Hyperelastic (Neo-Hooke)
GFRP	$E_{\parallel}$ = 42 000 MPa $E_{\perp}$ = 15 000 MPa $G_{\parallel,\perp}$ = 5 600 MPa $\nu_{\parallel,\perp}$ = 0.26	Linear elastic

E: Young's modulus; G: Shear modulus; G_0: Initial shear modulus; d: Incompressibility parameter; ν: Poisson's ratio

The resulting EPDM strains are expected to be comparatively large which is why a hyperelastic material model is utilized. Vasista et al. [27] tune the EPDM material parameters in ANSYS according to the results in [28] with the Neo-Hookean incompressible hyperelastic material model. The material properties used in this modeling are presented in table 2, based on the works of [27, 28] for EPDM and [25] for GFRP. Regarding EPDM, the physical relation of the incompressibility parameter d and the initial bulk modulus K is $K = 2/d$. Furthermore, since this work represents an early stage of the design, the values of G and ν for GFRP are not divided into parallel and perpendicular to the fiber orientation. However, in future studies, more detailed material parameters will be applied.

2.2 Setup of the FEA

As stated above, the FEA is build in ANSYS Workbench and the CAD model generation as well as the FE model generation is automatized. To facilitate sufficiently large deformations on the bump leading edge and trailing edge regions, EPDM is incorporated at these areas, extending

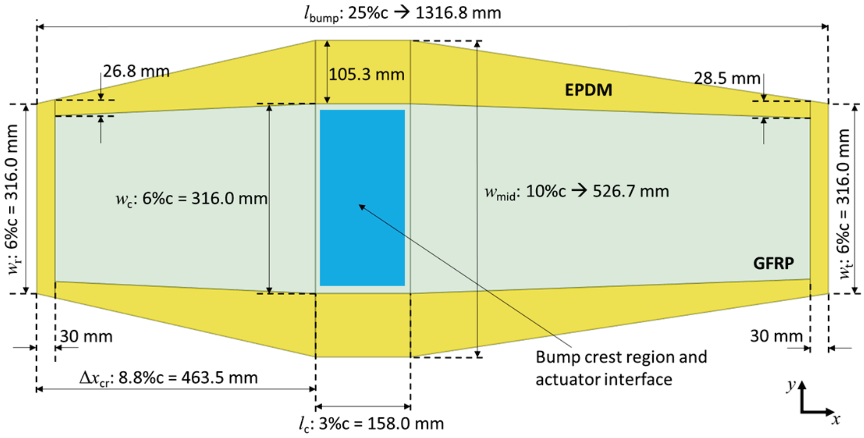

Figure 3: Top view of the 3D SCB model with EPDM (orange) and overall GFRP sections (light green) and GFRP interface for an actuator (blue), considered wing section chord length of 5 267 mm

30 mm in chordwise direction (x-direction). In addition, the bump side flanks are also made of EPDM, whereas the middle region is made of GFRP. This is depicted in figure 3.

The force respectively the displacement boundary condition to move the bump crest face (actuator interface) upwards can be set to different desired values of h_c. The underlying wing section has a chord length (c) of 5 267 mm. Thus, for the largest bump height in [17] of 1.15%c, the displacement condition is set to 60.6 mm. The outer edges of the EPDM have fixed boundary conditions, while an effective cruise pressure of -10 000 Pa is applied. This pressure represents an aerodynamic trade-off between lift and wave drag.

2.3 FEA simulation results for bump deployment

In the FEA, the GFRP thickness (t_{GFRP}) as well as the EPDM thickness (t_{EPDM}) are varied. The values of these studies are given in table 3. The initial baseline configuration of the morphing SCB structure is composed of t_{EPDM} = 30 mm and t_{GFRP} = 3 mm. The ply stacking is based on [25] with a single ply thickness of 0.125 mm. However, the 90° layer in the neutral axis which is present in [25] is neglected, in order to achieve an isotropic laminate stacking.

Table 3: Material thicknesses of the sensitivity studies

Parameter	Thicknesses (mm)
t_{GFRP}	3, 4, 5
t_{EPDM}	10, 20, 30, 40, 50

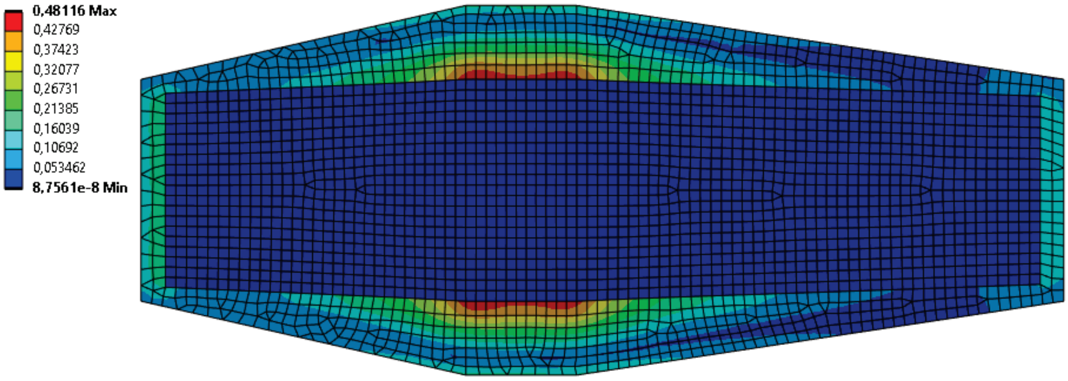

Figure 4: Top view of resulting equivalent von Mises strains (mm/mm) of EPDM and GFRP for 60.6 mm displacement (h_c = 1.15%c) and -10 000 Pa aerodynamic pressure load, t_{GFRP} = 3 mm, t_{EPDM} = 30 mm

In a first simulation of the baseline design, the displacement condition is set to the bump height of h_c = 1.15%c which corresponds to 60.6 mm. The resulting max. von Mises strains inside the GFRP reach 1.75% while the main deformation is covered by the EPDM which is strained by 48.12%. The combined strain results of EPDM and GFRP are depicted in figure 4, while the pure GFRP strain results can be found in figure 5. The results of all studies are summarized in table 4 at the end of chapter 2.5.

In light of extensive prior experience working with the GFRP used in this study, it is known that a maximum strain value of approximately 1% can be considered acceptable for this composite material. Upon examination of the GFRP results in figure 5 the comparatively high strains of about 1.75% are limited to the corners of the actuator interface. In contrast, the remaining structure displayes significantly lower strains. As such, reducing the corner strains is recommended for future work to ensure that the acceptable strain level of 1% is maintained. The overall structural concept, however, is deemed acceptable at this stage of design given these findings.

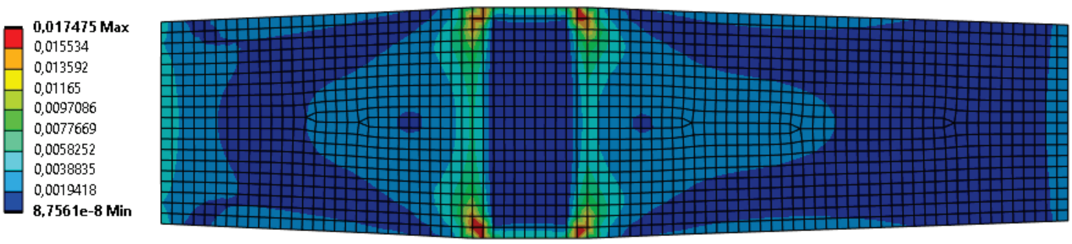

Figure 5: Top view of resulting equivalent von Mises strains (mm/mm) of the GFRP bump structure for 60.6 mm displacement (h_c = 1.15%c) and -10 000 Pa aerodynamic pressure load, t_{GFRP} = 3 mm, t_{EPDM} = 30 mm (EPDM is not shown)

Subsequently, t_{GFRP} is increased to 4 mm respectively 5 mm, while t_{EPDM} stays at 30 mm. The results in table 4 reveal that as the GFRP becomes thicker and consequently stiffer, the GFRP strains decrease but the EPDM strains increase. Taking into account all the studies carried out in this work, the maximum EPDM strains are 49.39% for the configuration with t_{GFRP} = 5 mm and t_{EPDM} = 30 mm.

Although EPDM can handle the resulting max. strains of approximately 50%, it is important to note that the Neo-Hookean material model is only valid for tensile strains up to 30-40% [29]. For larger strains, an alternative hyperelastic material model like the Odgen model may be more appropriate [30]. Therefore, it is recommended that the material model be revised or that the EPDM strains be reduced for future work to ensure accurate simulation results.

To investigate the impact of a smaller bump on the structural results, an additional simulation is performed with only 39.5 mm actuator interface z-displacement. This corresponds to h_c = 0.75%c since this height is also mentioned by Mayer et al. [17], even if not for the same design point and hence a slightly different SCB parametrization. However, for this smaller bump with t_{GFRP} = 3 mm and t_{EPDM} = 30 mm, the GFRP strains reach only 1.12% at the actuator interface corners and the EPDM is strained by only 29.01%.

2.4 FEA simulation results for clean cruise

As previously stated, when a flexible structure is subjected to aerodynamic pressure, it deforms. The challenge for morphing aircraft applications lies in designing a structure that is flexible enough to accommodate large deformations caused by actuation while being rigid enough to withstand operational loads. One important operating mode for such structures is the cruise with retracted bump, which maintains the clean airfoil shape. To achieve this, it is necessary to limit the contour deviations of the morphing skin due to cruise pressure to below 1 mm. To analyze this case, the actuator displacement is set to 0 mm, and the bump structure is loaded with

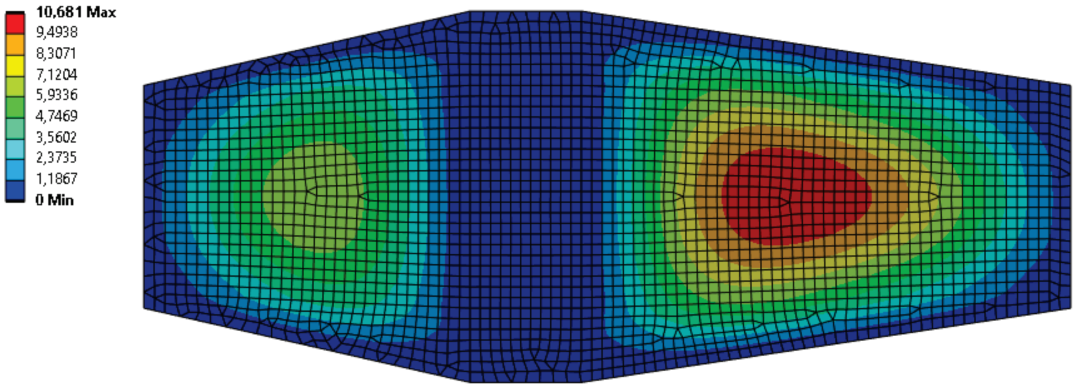

Figure 6: Top view of resulting deformations (mm) for 0 mm actuator interface displacement and -10 000 Pa aerodynamic pressure load, t_{GFRP} = 3 mm, t_{EPDM} = 30 mm

the previously mentioned average cruise pressure of -10 000 Pa. The deformation results for skin with 3 mm GFRP and 30 mm EPDM are shown in figure 6. They reveal a large deformation of approximately 10.7 mm of the morphing skin downstream of the actuator interface.

To see the effect of the EPDM thickness on aerodynamically-induced deformations, a sensitivity study is carried out for a constant GFRP thickness of 3 mm. Secondly, the GFRP thickness is varied for a constant EPDM thickness of 30 mm. The results of these two studies are depicted in figure 7. In this figure, the deformed center line is displayed. As depicted in figure 3, the major share of the center line belongs to the GFRP structure, while only 30 mm (in the x-direction) at the bump leading and trailing edges consist of EPDM.

The results shown in figure 7 emphasize a distinct influence of the EPDM thickness on the contour deviations. However, as t_{EPDM} increases, its impact on the contour deviations decreases. Thus, the relative differences of the deformations with t_{EPDM} of 30, 40 and 50 mm show minor divergences compared to the other EPDM thicknesses from 10 to 30 mm. Furthermore, the deformations in the downstream region are of same magnitude between the two configurations with t_{GFRP} = 3 mm and t_{EPDM} = 40 mm and the one with t_{GFRP} = 4 mm and t_{EPDM} = 30 mm. A similar behavior is observed in the downstream region for t_{GFRP} = 5 mm with t_{EPDM} = 30 mm and t_{GFRP} = 3 mm with t_{EPDM} = 50 mm. These findings suggest that designers have the flexibility to achieve comparable results using various combinations of GFRP and EPDM thicknesses.

However, even for the thickest simulated GFRP structure (t_{GFRP} = 5 mm, t_{EPDM} = 30 mm) the z-deformations respectively contour deviations are 3.8 mm upstream and 7.0 mm downstream of the actuator interface. Consequently, a new approach has to be considered to decrease the contour deviations in clean configuration below the target of 1 mm.

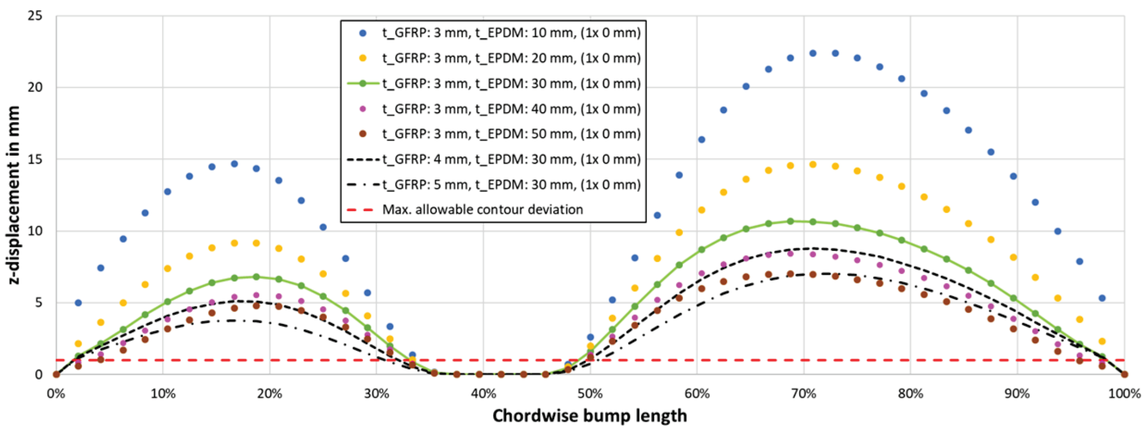

Figure 7: Deformations in z-direction of the center line (mm) for varying EPDM thicknesses, with 0 mm actuator displacement and -10 000 Pa aerodynamic pressure load

2.5 Additional actuators

Due to this fact, that the aerodynamic cruise pressure deforms the morphing structure too much a solution must be found to overcome this drawback. One approach could be to actively control the pressure below the flexible bump structure as already done in [5, 6, 7, 21, 24]. Another idea is to implement several actuation points upstream and downstream of the bump crest face. A similar approach can be found in [3, 4]. Additional actuators could be used not only to change the bump crest position in chordwise direction, but also to achieve an improved shape control on the bump upstream ramp and downstream tail. However, in the following study, the additional actuator interfaces are used to hold the structure down against aerodynamic loads.

In figure 8, the baseline configuration (t_{GFRP} = 3 mm, t_{EPDM} = 30 mm) is further equipped with one respectively two additional actuators (displacement conditions of 0 mm) downstream of the main bump crest actuator interface (Act. 1). Furthermore, a fourth actuator is placed on the upstream ramp. The results reveal that with the implementation of a second actuator downstream of the main actuator, the largest deformation due to the aerodynamic pressure occurs on the upstream ramp. Consequently, the maximum deformations of the simulations with two and three actuators are identical (6.8 mm) as shown in table 4. Only with the addition of an actuator on the upstream ramp, it is possible to reduce these deformations.

Figure 8 clearly shows that more actuators reduce the contour deviations of the skin under aerodynamic loading, as expected. With four actuator interfaces, the center line contour deviations under aerodynamic loading are less than 1 mm, compared to the clean, unloaded wing shape. Nevertheless, the center line plot in figure 8 gives mainly an impression of the GFRP deformations, while the largest shares of EPDM are implemented on the bump side flanks. Therefore, figure 9 depicts the overall deformations, including these EPDM regions for the four-actuator configuration.

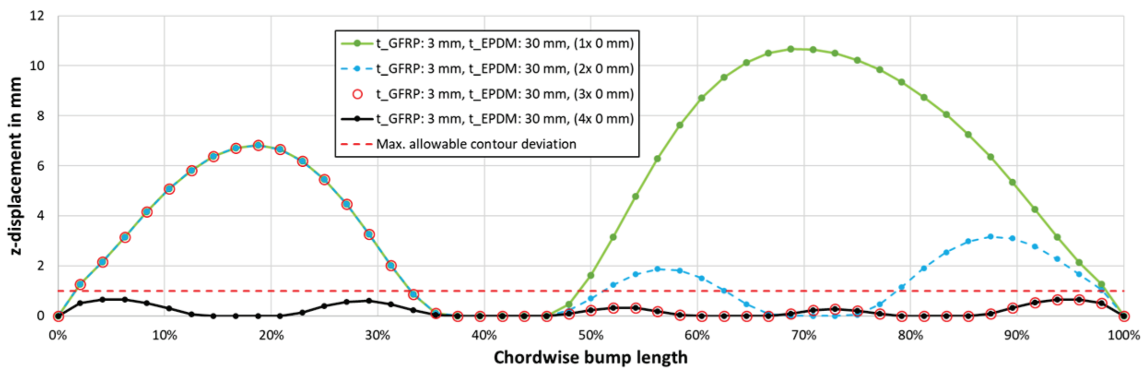

Figure 8: Deformations (mm) in z-direction of the center line with 0 mm displacement at up to four actuator interfaces, with -10 000 Pa aerodynamic pressure load, t_{GFRP} = 3 mm, t_{EPDM} = 30 mm

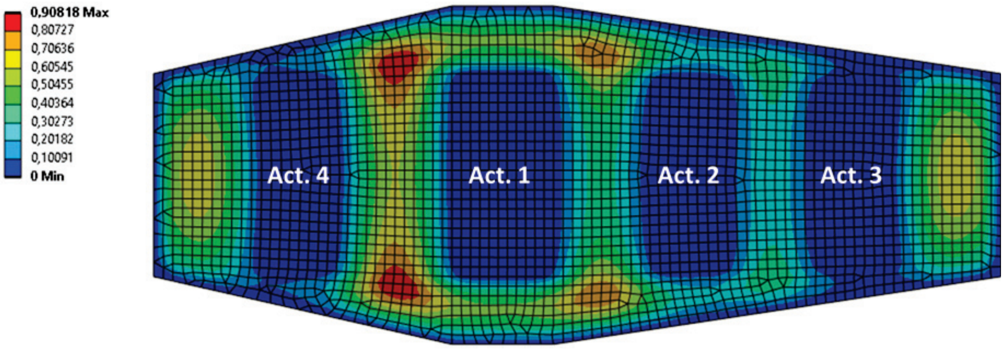

Figure 9: Top view of the total deformations (mm) with 0 mm displacement at four actuator interfaces for -10 000 Pa aerodynamic pressure load, t_{GFRP} = 3 mm, t_{EPDM} = 30 mm

These results show maximum deformations of about 0.9 mm on the side flanks close to the main actuator interface. Even in these highly flexible EPDM regions, deformations due to aerodynamic pressure loading in clean configuration remain within the contour limit of 1 mm.

In table 4, not only the resulting deformations and strains of the morphing structure are presented, but also the actuator forces. A positive value indicates that the main actuator has to push the structure in positive z-direction to deploy the SCB. Negative values represent a pulling

Table 4: FEA results of deformations, strains and actuator forces for an aerodynamic pressure load of -10 000 Pa, t_{EPDM} = 30 mm

Simulation Setup			Results						
t_{GFRP} (mm)	Act. displ. (mm)	Bump height (%c)	Max. deform. (mm)	Max. GFRP strain	Max. EPDM strain	Act. 1 force (N)	Act. 2 force (N)	Act. 3 force (N)	Act. 4 force (N)
3	21.0	0.40	21.1	0.61%	14.46%	1 332	-	-	-
3	39.5	0.75	39.5	1.12%	29.01%	6 891	-	-	-
3	60.6	1.15	60.6	1.75%	48.12%	17 430	-	-	-
4	60.6	1.15	60.6	1.55%	48.91%	18 928	-	-	-
5	60.6	1.15	60.6	1.42%	49.39%	20 473	-	-	-
3	1x 0	-	10.7	0.21%	6.55%	-1 892	-	-	-
3	2x 0	-	6.8	0.18%	5.13%	-2 120	-2 247	-	-
3	3x 0	-	6.8	0.18%	5.13%	-1 829	-972	-852	-
3	4x 0	-	0.9	0.08%	1.08%	-1 325	-972	-853	-1 015

t: thickness (in z-direction); GFRP: glass-fiber reinforced polymer; EPDM: ethylene propylene diene monomer; Act.: actuator; displ.: displacement; deform.: deformation; FEA: finite element analysis force required to hold the structure in clean configuration against the aerodynamic pressure. The forces to deploy the bump with a height of h_c = 1.15%c are comparatively large. However, since the installation space beneath the skin is limited, the actuators should be minimized in size, which in general corresponds to lower forces. Therefore, thinner GFRP laminates are recommended to reduce actuator loads during bump deployment. Additionally, reducing the bump height from 1.15%c (corresponding to a deformation of 60.6 mm) to 0.75%c (resulting in a displacement of 39.5 mm) would lead to distinctly smaller strains and actuator forces. Furthermore, when the bump height is reduced to 0.40%c (corresponding to 21 mm), the force of actuator 1 amounts only to 1.3 kN. This comparatively small force arises primarily because most of the deformation is caused by aerodynamic pressure. Hence, if in future work an aero-structural SCB optimization is realized the bump height could be reduced to values that are still aerodynamically efficient, and at the same time leading to actuator forces and structural loads that stay in acceptable magnitudes.

3 CONCLUSION AND OUTLOOK

In this work, a novel structural design of a morphing 3D shock control bump has been introduced. By combining fiberglass composite laminates with regions of highly flexible elastomer, large deformations are enabled. While the middle region of the bump structure is made of GFRP, the side flanks as well as small regions at the bump leading and trailing edges are composed of EPDM. Three different GFRP thicknesses (3 mm, 4 mm and 5 mm) have been investigated through finite element analyses, with the EPDM thickness varying from 10 mm to 50 mm. The morphing structure is loaded with a suction pressure of -10 000 Pa representing aerodynamic loading during cruise. While displacement conditions correspond to actuators in current simulations, detailed actuator designs should be investigated in future work.

In addition to the bump deployment, the focus of this works lies on the clean configuration with retracted bump. Since one single actuator has been found to be not sufficient to hold the morphing structure against aerodynamic loading in acceptable limits of the contour deviations, the application of up to four actuators is investigated. For the baseline structure, which has thicknesses of 3 mm GFRP and 30 mm EPDM, four actuators would lead to contour deviations of less than 1 mm during cruise. Future designs may incorporate varying GFRP thicknesses along the bump chord to achieve sufficient stiffness, potentially requiring only one additional downstream actuator. Conversely, employing multiple actuators could enhance contour accuracy and facilitate the use of comparatively thin GFRP structures.

In future work, the morphing concept will be explored by using several actuators to vary the bump crest location in chordwise direction, enabling adaptation to changes in transonic shock position. The GFRP strain concentrations on the four corners of the actuator interface will be reduced, e.g. by implementing an elliptical shape of the interface, or by locally optimizing the structural design. More detailed structural analyses considering laminate failure criteria are planned. Additionally, the bump flank angles should be evaluated with respect to aerodynamic targets. Moreover, not only the max. contour deviations but also the waviness should be taken into consideration. Furthermore, a comprehensive actuator design study will be conducted in conjunction with evaluating the available design space. This includes the analysis of whether the aerodynamic pressure alone could be sufficient to lift the flexible skin and form an accurate bump shape. If so, only an actuation to pull the bump down to clean configuration would be required. Finally, the precise placement of the SCB will presumably necessitate its implementation between the wing spars, requiring a redesign of the load-bearing upper wing skin.

4 ACKNOWLEDGMENT

This work is part of the DLR project LamTA. Special thanks go to Thomas Kilian for consulting in aerodynamic questions and Srinivas Vasista regarding morphing structures.

References

[1] K. Hainsch, L. Göke, C. Kemfert, P.-Y. Oei, and C. V. Hirschhausen, "European green deal: Using ambitious climate targets and renewable energy to climb out of the economic crisis," *DIW Weekly Report*, vol. 10, pp. 303–310, 2020. [Online]. Available: https://doi.org/10.18723/DIW_DWR:2020-28-1

[2] A. Krein and G. Williams, "Flightpath 2050: Europe's vision for aeronautics," in *Innovation for Sustainable Aviation in a Global Environment: Proceedings of the Sixth European Aeronautics Days*, D. Knörzer and J. Szodruch, Eds., vol. 30, 2012, pp. 63–71, Madrid, Spain. [Online]. Available: https://doi.org/10.3233/978-1-61499-063-5-63

[3] T. Bein, H. Hanselka, and E. Breitbach, "An adaptive spoiler to control the transonic shock," *Smart Materials and Structures*, vol. 9, no. 2, pp. 141–148, 04 2000. [Online]. Available: https://www.doi.org/10.1088/0964-1726/9/2/303

[4] L. F. Campanile, R. Keimer, and E. J. Breitbach, "The "fish-mouth" actuator: Design issues and test results," *Journal of Intelligent Material Systems and Structures*, vol. 15, no. 9, pp. 711–719, 09 2004. [Online]. Available: https://www.doi.org/10.1177/1045389X04044452

[5] M. Kintscher, N. Alves de Sousa, H. P. Monner, and M. Wiedemann, "Generation of a shock control bump by pressurized chambers," in *26th International Conference on Adaptive Structures and Technologies (ICAST2015)*, 10 2015, Kobe, Japan. [Online]. Available: https://elib.dlr.de/100017/

[6] N. B. L. Alves de Sousa, "Design of an adaptive shock control bump using pressurized chambers - structural realization, actuation and integration," 06 2017, Master's thesis, University Técnico Lisboa. [Online]. Available: https://fenix.tecnico.ulisboa.pt/cursos/meaer/dissertacao/283828618790088

[7] N. Alves de Sousa, M. Kintscher, and A. Suleman, “Morphing of an adaptive shock control bump using pressurized chambers,” *Journal of Intelligent Material Systems and Structures*, 06 2020. [Online]. Available: https://www.doi.org/10.1177/1045389X20932214

[8] S. C. Künnecke, M. Schäfer, A. Goerttler, A. Waldmann, S. Vasista, and J. Riemenschneider, “CONCEPT OF A MORPHING SHOCK CONTROL BUMP SPOILER WITH TWO ACTUATORS,” in *10th ECCOMAS Thematic Conference on Smart Structures and Materials*. Dept. of Mechanical Engineering & Aeronautics University of Patras, 07 2023, pp. 291–302, Patras, Greece. [Online]. Available: https://www.doi.org/10.7712/150123.9786.441212

[9] S. C. Künnecke, J. Riemenschneider, and H. P. Monner, “Adaptive shock control bump with shape memory alloy wires on a morphing spoiler,” in *ASME 2024 Conference on Smart Materials, Adaptive Structures and Intelligent Systems*, 09 2024, V001T04A003, Atlanta, Georgia, USA. [Online]. Available: https://www.doi.org/10.1115/SMASIS2024-139102

[10] S. Barbarino, O. Bilgen, R. M. Ajaj, M. I. Friswell, and D. J. Inman, “A review of morphing aircraft,” *Journal of Intelligent Material Systems and Structures*, vol. 22, no. 9, pp. 823–877, 06 2011. [Online]. Available: https://doi.org/10.1177/1045389X11414084

[11] E. Stanewsky, “Aerodynamic benefits of adaptive wing technology,” *Aerospace Science and Technology*, vol. 4, no. 7, pp. 439–452, 10 2000. [Online]. Available: https://doi.org/10.1016/S1270-9638(00)01069-5

[12] A. Goerttler, “Aerodynamic design of shock control bumps on a transport aircraft wing considering structural constraints,” in *AIAA SCITECH 2024 Forum*. American Institute of Aeronautics and Astronautics, 01 2024, Orlando, FL. [Online]. Available: https://doi.org/10.2514/6.2024-2133

[13] J. P. Eastwood and J. P. Jarrett, “Toward designing with three-dimensional bumps for lift/drag improvement and buffet alleviation,” *AIAA Journal*, vol. 50, no. 12, pp. 2882–2898, 12 2012. [Online]. Available: https://arc.aiaa.org/doi/10.2514/1.J051740

[14] A. Waldmann, J. Müller, A. Goerttler, and T. Lutz, “Shock control bumps for buffet onset delay on sections of a wing with hybrid laminar flow control,” in *New Results in Numerical and Experimental Fluid Mechanics XIV*, A. Dillmann, G. Heller, E. Krämer, C. Wagner, and J. Weiss, Eds. Springer Nature Switzerland, 2024, vol. 154, pp. 693–703. [Online]. Available: https://doi.org/10.1007/978-3-031-40482-5_65

[15] P. R. Ashill, J. L. Fulker, and A. Shires, “A novel technique for controlling shock strength of laminar-flow aerofoil sections,” in *First European Forum on Laminar Flow Technology*, 03 1992, pp. 175–183, Hamburg, Germany.

[16] A. Goerttler, S. C. Künnecke, and C. Sabater, “Aerodynamic design of shock control bumps considering structural constraints,” in *New Results in Numerical and Experimental Fluid Mechanics XIV*, A. Dillmann, G. Heller, E. Krämer, C. Wagner, and J. Weiss, Eds. Springer Nature Switzerland, 2024, vol. 154, pp. 671–681. [Online]. Available: https://doi.org/10.1007/978-3-031-40482-5_63

[17] R. Mayer, T. Lutz, and E. Krämer, “Numerical study on the ability of shock control bumps for buffet control,” *AIAA Journal*, vol. 56, no. 5, pp. 1978–1987, 05 2018. [Online]. Available: https://doi.org/10.2514/1.J056737

[18] P. J. K. Bruce and S. P. Colliss, “Review of research into shock control bumps,” *Shock Waves*, vol. 25, no. 5, pp. 451–471, 09 2015. [Online]. Available: https://doi.org/10.1007/s00193-014-0533-4

[19] H. Ogawa, H. Babinsky, M. Pätzold, and T. Lutz, “Shock-wave/boundary-layer interaction control using three-dimensional bumps for transonic wings,” *AIAA Journal*, vol. 46, no. 6, pp. 1442–1452, 06 2008. [Online]. Available: https://doi.org/10.2514/1.32049

[20] O. Rhodes and M. Santer, “Structural optimization of a morphing shock control bump,” in *52nd AIAA/ASME/ASCE/AHS/ASC Structures, Structural Dynamics and Materials Conference*, vol. AIAA 2011-2129. American Institute of Aeronautics and Astronautics, 04 2011, pp. 6039–6056, Denver, Colorado, USA,. [Online]. Available: https://doi.org/10.2514/6.2011-2129

[21] M. Gramola, P. J. Bruce, and M. Santer, “Passive control of 3d adaptive shock control bumps using a sealed cavity,” *Journal of Fluids and Structures*, vol. 112, p. 103580, 07 2022. [Online]. Available: https://doi.org/10.1016/j.jfluidstructs.2022.103580

[22] M. Kintscher, J. Riemenschneider, H.-P. Monner, and M. Wiedemann, “Structural concept of an adaptive shock control bump spoiler,” *CEAS Aeronautical Journal*, vol. 12, no. 3, pp. 509–518, 08 2021. [Online]. Available: https://www.doi.org/10.1007/s13272-021-00507-9

[23] S. C. Künnecke, S. Vasista, J. Riemenschneider, R. Keimer, and M. Kintscher, “Review of adaptive shock control systems,” *Applied Sciences*, vol. 11, no. 2, p. 817, 01 2021. [Online]. Available: https://doi.org/10.3390/app11020817

[24] E. R. Jinks, P. J. Bruce, and M. J. Santer, “The use of actuated flexible plates for adaptive shock control bumps,” in *53rd AIAA Aerospace Sciences Meeting*, ser. AIAA SciTech Forum. American Institute of Aeronautics and Astronautics, 01 2015, Kissimmee, Florida, USA. [Online]. Available: https://doi.org/10.2514/6.2015-1241

[25] S. Vasista, F. Nolte, H. P. Monner, P. Horst, and M. Burnazzi, “Three-dimensional design of a large-displacement morphing wing droop nose device,” *Journal of Intelligent Material Systems and Structures*, vol. 29, no. 16, pp. 3222–3241, 09 2018. [Online]. Available: https://www.doi.org/10.1177/1045389X18770863

[26] M. Radestock, A. Falken, J. Riemenschneider, and M. Kintscher, “Hybrid skin design of the transition region between morphing wing and fixed wing,” in *Proceedings of the ASME 2018 Conference on Smart Materials, Adaptive Structures and Intelligent Systems. Volume 1: Development and Characterization of Multifunctional Materials; Modeling, Simulation, and Control of Adaptive Systems; Integrated System Design and Implementation.*, 09 2018, V001T04A013, San Antonio, Texas, USA. [Online]. Available: https://www.doi.org/10.1115/SMASIS2018-7976

[27] S. Vasista, F. Nolte, M. Schäfer, and J. Riemenschneider, “Design and manufacture of a fluid-actuated morphing winglet trailing edge control surface,” in *ASME 2022 Conference on Smart Materials, Adaptive Structures and Intelligent Systems (SMASIS)*, 09 2022, V001T04A013, Dearborn, Michigan, USA. [Online]. Available: https://www.doi.org/10.1115/SMASIS2022-91054

[28] K. Jacobi, “Aufbau einer regelung für die verformung von morphenden flügelhinterkanten,” 2021, Master’s thesis, Otto-von-Guericke-Universität, Magdeburg, Germany. [Online]. Available: https://elib.dlr.de/146878/

[29] ANSYS Inc., “ANSYS mechanical advanced nonlinear materials - hyperelasticity - appendix 4a,” 03 2017. [Online]. Available: https://innovationspace.ansys.com/courses/wp-content/uploads/sites/5/2024/01/8_Modulus-vs-Strain-data.pdf

[30] B. Kim, S. B. Lee, J. Lee, S. Cho, H. Park, S. Yeom, and S. H. Park, “A comparison among Neo-Hookean model, Mooney-Rivlin model, and Ogden model for chloroprene rubber,” *International Journal of Precision Engineering and Manufacturing*, vol. 13, no. 5, pp. 759–764, 05 2012. [Online]. Available: https://www.doi.org/10.1007/s12541-012-0099-y